Self-Immolative Polymers with Potent and Selective Antibacterial Activity by Hydrophilic Side Chain Grafting

Cansu Ergene and Edmund F. Palermo*

Department of Materials Science and Engineering, Rensselaer Polytechnic Institute, 110 8th St., Troy, New York 12180, USA

*Email: palere@rpi.edu

Abstract. We report the first example of a self-immolative polymer that exerts potent antibacterial activity combined with relatively low hemolytic toxicity. Specifically, self-immolative poly(benzyl ether)s bearing pendant cationic ammonium groups and grafted poly(ethylene glycol) chains in the side chains were prepared via post-polymerization thiol-ene chemistry. These functional polymers undergo sensitive and specific triggered depolymerization into small molecules upon exposure to a designed stimulus (in this example, fluoride ion cleaves a silyl ether end cap). The molar composition of the resulting statistical copolymers was varied from 0 to 100% PEG side chains. The average molar mass of the pendant PEG chains was either 800 or 2000 g/mol. The antibacterial and hemolytic activities were evaluated as function of copolymer composition. Strong bactericidal activity (low μg/mL MBC) was retained in copolymers containing 25 – 50% PEG-800, whereas hemolytic toxicity monotonically decreased (up to HC_{50} >1000 μg/mL) with increasing PEG content. PEG-2000 was far less effective; both the MBC and HC_{50} decreased to a comparable extent with increasing PEGylation. Overall, the best cell type selectivity index (HC_{50}/MBC ~ 28) was obtained for the copolymer containing ~ 50% cysteamine and ~50% PEG-800 side chains, as compared to the cationic homopolymer (HC_{50}/MBC < 1). Thus, systematic tuning of PEG graft density and chain length effectively enhances the cell-type selectivity of these self-immolative polymers by orders of magnitude.

Introduction

The alarmingly rapid proliferation of antibiotic-resistance bacterial infections, compounded by the continuously declining number of new antibiotic drug approvals, is a global health crisis. The urgency of this problem has led many researchers to seek new antibacterial agents[1-3]. Host defense peptides (HDPs) are components of innate immunity that exert antibacterial efficacy with minimal toxicity to host cells[4-6]. Synthetic mimics of HDPs including β-peptides[7], peptoids[8], nylon-3 copolymers[9], polymethacrylates[10-12], polymethacrylamides,[13] polycarbonates[14-17] and polynorbornenes[18-20], are designed to capture the essential physiochemical features of the peptides: cationic charge, hydrophobicity, and short chain length.[21-24] HDPs and their synthetic mimics are widely thought to exert a mechanism of action involving membrane disruption[25, 26] and are less likely to induce bacterial resistance as compared to conventional antibiotic drugs[27]. Still, HDPs are expensive to manufacture and are rapidly degraded by proteases *in vivo*[28], which motivates the continued development of biomimetic synthetic polymers.[29-31]

In contrast to the proteolytic instability of HDPs, vinyl-based synthetic antibacterial polymers do not degrade appreciably in physiological conditions. Their chemical stability may restrict biomedical use due to long-term toxicity *in vivo*, even if they are non-toxic in short-term *in vitro* studies[17, 32]. Thus, biodegradable antibacterial polymers such as polyesters[32, 33], polycarbonates[15, 34] and even acetal networks[35] are of increasingly high interest. These polymers are subject to cleavage at random sites along the backbone of the polymer chains, thus representing a passive degradation rate that is dictated by the chemical structure of the linkage and the solvent-accessibility of the microenvironment[36]. In contrast to conventional biodegradable polymers, metastable "self-immolative" polymers (SIMPs) undergo triggered end-to-end depolymerization

in response to a specific stimulus.[37] Upon the cleavage of a labile ω-end-cap, above the ceiling temperature T_c, the active species of depropagation is liberated and the chain will spontaneously unzip into its component monomers.[38-41] This unique phenomenon provides marked signal amplification, as well as mechanical transduction of chemical signals, and the unparalleled specificity to control the onset of chemical degradation (rather than simply tuning the passive release profile). SIMPs have been used in applications of drug delivery[42-44], biosensors[45], microfluidics[46] and dynamically recyclable plastics[47, 48] but were not utilized in antimicrobial platforms until very recently. In the context of antibacterial materials development, self-immolation provides a unique opportunity to trigger the conversion from polymer to small molecule, which dramatically alters the mechanical properties and solubility characteristics of the material, on demand. One may envision application in "smart" bio-responsive coatings that mediate triggered release of biologically active small molecules into the surrounding media.

We recently reported the first example of a biocidal self-immolative polymer[49] based on modifcations to the poly(benzyl ether) (PBE) platform pioneered by Phillips and co-workers.[50, 51] The cationic PBEs bearing primary amine groups displayed rapid, broad-spectrum antibacterial activity and were readily depolymerized into small molecules upon introduction of chemical "trigger". However, these first-generation cationic PBEs are also highly toxic to red blood cells (RBCs). We hypothesized that the intensely hydrophobic nature of the PBE backbone leads to the high hemolytic toxicity and limits aqueous solubility. In this work, we present a simple PEGylation strategy to decrease the overall hydrophobicity of the PBEs and thus reduce the hemolytic toxicity, while retaining the antibacterial potency.

The classical approach to HDP-mimetic design involves optimization of two key features in a polymer structure: the cationic charge and the hydrophobicity. However, binary copolymers

were found to contain both higher cationic charge density and higher hydrophobicity than the average HDP.[52] It is clear that HDPs are not solely composed of cationic and hydrophobic residues, but also contain an abundance of neutral, hydrophilic groups. Consequently, ternary copolymer systems containing neutral, hydrophilic groups (hydroxyls,[53, 54] sugars,[55, 56] Zwitterions, [57] PEG[58, 59]) have been studied. Incorporation of the third component played an important role in modulating the cell-type selectivity of a polymer by reducing the hemolytic toxicity while maintaining (or even improving) the antibacterial efficacy. Youngblood and co-workers reported[60] ternary antimicrobial copolymers of hydrophobically quaternized 4-vinyl pyridine (4VP) with PEG methacrylate. Compared to highly antibacterial and hemolytic quaternized PVP, the PEGylated copolymers exhibited lower hemolytic toxicity and their retained antibacterial activity.[60]

In this paper, we modified cationic PBEs with varying content of PEG grafts in the side chains to quantify the effects of reducing hydrophobicity on the antibacterial and hemolytic activities. Poly (benzyl ether)s with allyl side chains and silyl ether end-caps were synthesized based on modifications to the route recently described by Phillips and co-workers[50]. Relative to the first-generation cationic PBEs, the PEGylated variants exhibited lower hemolytic toxicity while maintaining comparable level of antibacterial potency. The best example showed a 28-fold selectivity toward *E. coli* over red blood cells, which is a remarkable improvement over our first-generation biocidal SIMPs, which gave a selectivity index of < 1.

Results and Discussion

Polymer Synthesis. We prepared a library of PBEs with PEGylated and cationic side chains, in various copolymer ratios and with two different PEG chain lengths (Figure 1). Briefly, anionic

polymerization was carried out at -20 °C in THF, which is below the ceiling temperature of PBE ($T_c \sim 0$ °C at 1M), followed by end-capping with TBDMS-Cl, to give the pre-polymer $\mathbf{P_0}$. The monomer:initiator ratio was fixed at 10:1 in all polymerizations to give short oligomers, because previous work has shown this chain length regime to be the most promising for nontoxic antibacterials.

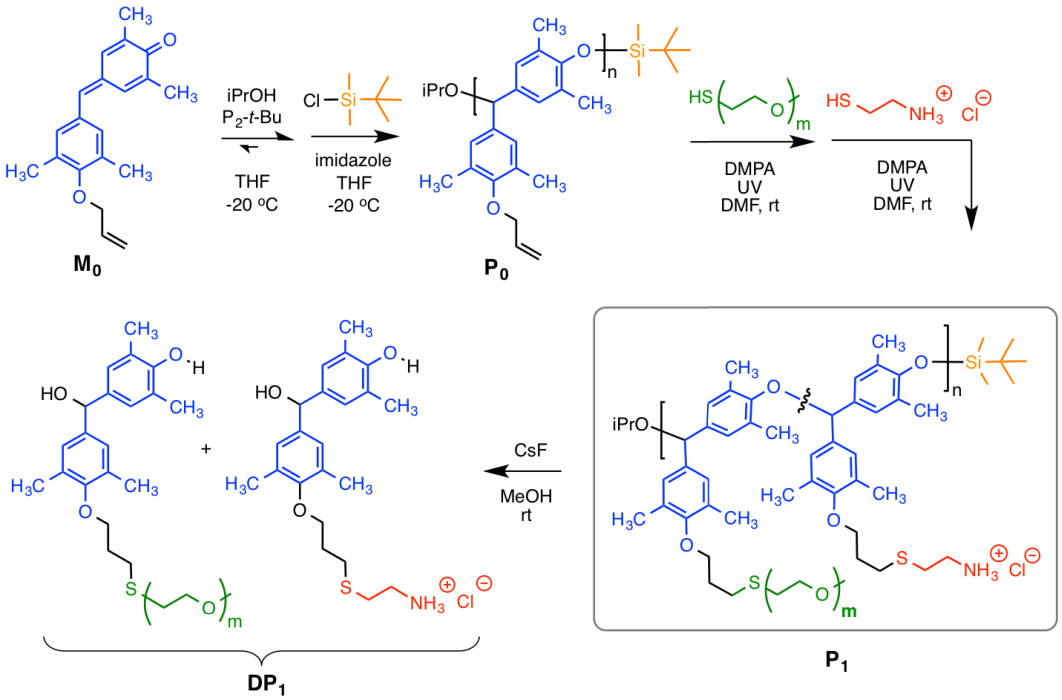

Figure 1. General scheme for the synthesis of self-immolative antibacterial polymers with pendant PEG and ammonium groups: low-temperature anionic polymerization of a quinone methide monomer, end-capping, post-polymerization thiol−ene functionalization, and chemically triggered depolymerization with fluoride.

We obtained PBEs with the number-average molecular weights in the range of M_n = 3.4 − 3.6 kDa with dispersities of Đ = 1.42 − 1.57 by GPC. The moderately broad dispersities observed here are comparable to previous reports on related polymerizations by Phillips[50] and our group.[49] Although the "livingness" of this polymerization has not been examined mechanistically to date, there are two reasonable hypotheses regarding the cause of MWD broadness; either chain transfer or equilibration of the propagation and depropagation processes

following complete conversion. Similar M_n values were found by ^{1}H NMR end-group analysis (see Supporting Information). The side chains of **P_0** are allyl-functionalized for further modification.

The goal of this study was to incorporate neutral, hydrophilic functionality into self-immolative polymers to confer antibacterial activity with minimal hemolytic toxicity. To that end, the allyl side chains of the pre-polymer **P_0** were functionalized with cysteamine HCl (the thiol obtained by cleavage of the disulfide bond in cystamine HCl) and PEG methyl ether thiol (PEG-SH $M_n \sim 800$ Da or 2 kDa) via thiol-ene radical addition. The UV photoiniator Irgacure 651 was employed under irradiation of a handheld UV lamp (6W, 365 nm) for 10 min at room temp. In order to control the ratio of PEG and primary amines in the side chains, we first functionalized a fraction of the allyl side groups with PEG thiols, confirmed the partial conversion by ^{1}H NMR (see data in ESI), and then proceeded to functionalization of the remaining unreacted allyl groups with excess cysteamine HCl. Each copolymer was purified by preparative size exclusion chromatography on LH-20 gel in MeOH. Copolymer compositions and number-average chain lengths were quantified by ^{1}H NMR for the final copolymer products (Figure 2). See the SI for spectra of all polymers. We successfully obtained graft copolymers across the full range of copolymer compositions (from 0 to 100 mol% PEG). In all cases, the observed copolymer composition is in good agreement with the target values (data in ESI).

All of the functionalized copolymers dissolve in polar solvents such as MeOH, DMF and DMSO. Whereas the copolymers containing 0-33% PEG_{800} are not soluble in aqueous buffers, the copolymers with 50% or more PEG_{800} in side chains demonstrated facile water solubility (up to 1 mg/mL). This observation is consistent with the idea that PEGylation alleviates the intense hydrophobicity of the PBE scaffold. Each copolymer was serially diluted in 2-fold increments

from a DMSO stock solution (20 mg/mL) into aqueous buffers to give final polymer concentrations in the µg/mL range, which is the desired range for our biological assays. As a control experiment, we confirmed that the residual amount of DMSO (maximum 5% v/v in assay condition) had no significant effect on bacterial cell viability or on hemolytic activity.

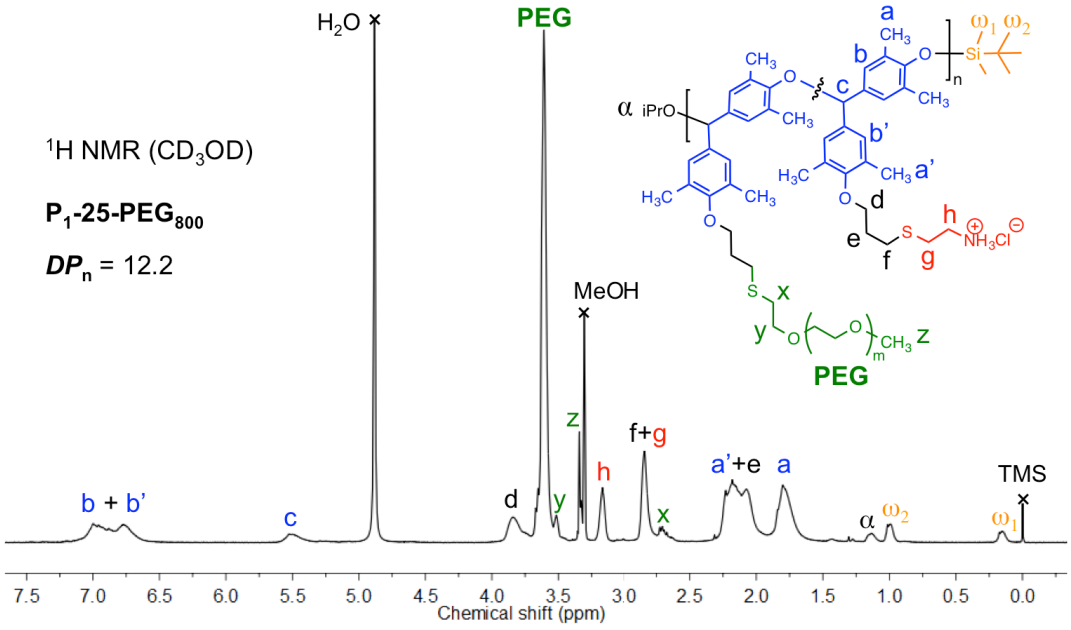

Figure 2. ^{1}H NMR spectrum (CD_3OD) of **P_1-25-PEG_{800}**. Copolymer composition and degree of polymerization are calculated based on the ratios of integrated peak areas.

Dye-Labeled Polymers. We also prepared PBEs end-capped with Rhodamine NHS ester, in order to enable their observation by confocal fluorescence microscopy (Figure 5A and B), as well as to aide in quantification of the water-octanol partition coefficients [logP = $\log([\text{polymer}]_{octanol} / [\text{polymer}]_{water})$], a standard measure of hydrophobicity that is widely used as a metric in structure-activity relationship (SAR) studies. Positive logP values indicate a preference for solubility in octanol, whereas negative values indicate preference for the water phase. These dye labeled polymers were functionalized with cysteamine and PEG-SH in various

ratios (0, 50, and 100% PEG) by the same methods as above. Our hypothesis was that PEGylation would reduce the overall hydrophobicity of the copolymers. Indeed, the logP values exhibit a marked dependence on PEG fraction. The logP values for copolymer containing 0, 50, and 100% PEG_{800} in the side chains are +0.26, −0.56, and −1.20, respectively (Figure 3). Thus, the hydrophobicity trend is quite clear: increasing the PEG content leads to markedly increased hydrophilicity in the copolymers, which strongly supports of the central hypothesis driving this work. Encouraged by this result, we proceeded to perform SAR studies on this class of polymers.

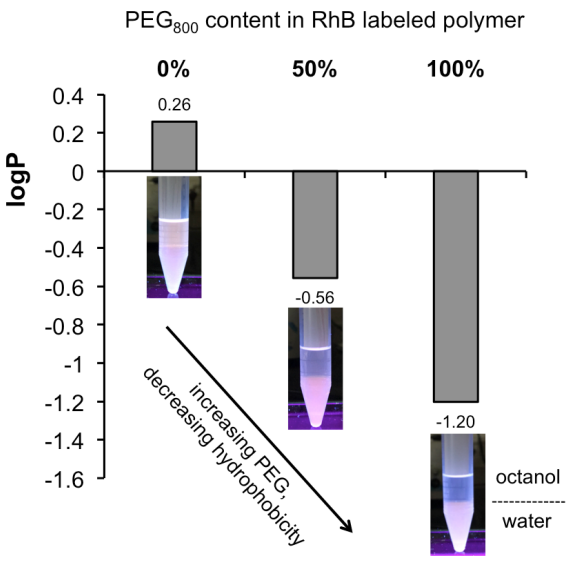

Figure 3. Water-octanol partition coefficients (logP) for the Rhodamine-labeled polymers with 0, 50, and 100% PEG_{800} in the side chains.

Bactericidal activity. The minimum bactericidal concentration (MBC) is defined here as the lowest polymer concentration required to induce at least a 3-log reduction in the number of viable *E. coli* cells in PBS buffer after 90 min incubation at 37 °C. We quantified the effect of PEGylation extent, as well as the length of the pendant PEG chains, on bactericidal activity (Table 1 and Figure 4). The cationic homopolymer, bearing 100% primary ammonium side chains (**P_1-0**), exhibited potent bactericidal action against *E. coli* with a MBC of 12 μg/mL, which is similar to the MBC of the bee venom toxin peptide melittin (MBC = 4 μg/mL) in the same assay conditions. In our earlier study, we reported similar polymers as strong bactericides with a high degree of cationic charge and hydrophobicity via surfactant-like mode of action.

To dilute the high degree of cationic charge and partially screen the hydrophobicity of the

PBE backbone, we grafted hydrophilic PEG chains onto a fraction of the PBE side chains. Incorporation of modest amounts of PEG_{800} (11 and 25 mol %) did not significantly alter the antibacterial potency, with MBC values of 26 μg/mL. Further increasing the PEG content (33 and 50 mol %) resulted in MBC values of 12 μg/mL, which is unchanged relative to the cationic homopolymer. Although PEGylation reduces the hydrophobicity and cationic charge of the copolymers, the improved aqueous solubility of the PEGylated copolymers is a countervailing effect that may offset the reduced electrostatic interaction with bacterial membranes[61]. Further increases in the PEG_{800} content (beyond 50%) lead to a dramatic loss of antibacterial potency; the copolymer with 57 mol% PEG_{800} has a modest MBC value of 219 μg/mL and those with 63 mol% or higher do not measurably kill *E. coli* even at the highest concentration tested (1000 μg/mL).

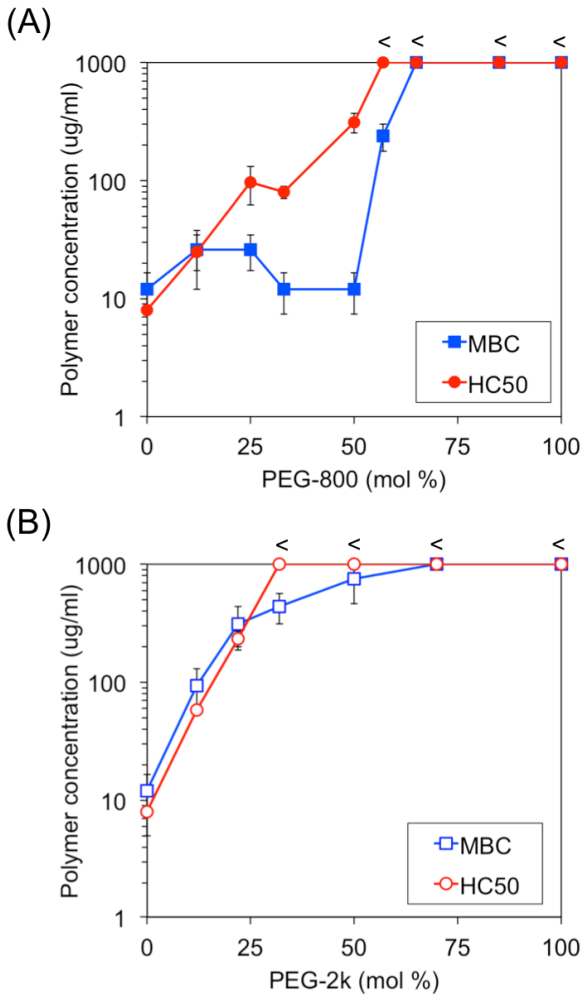

Figure 4. Antibacterial activity and hemolytic activities of polymers with varying mole % of (A) PEG-800 and (B) PEG-2k, as a function of PEG content.

The size effect of grafted PEG chains on antibacterial activity is rather pronounced. When PEG_{2k} is employed instead of PEG_{800}, the antibacterial potency decreases monotonically with increasing PEG content across the entire range of copolymer compositions (0-100%). Inclusion

of just 12 mol% PEG_{2k} in side chains caused an increase in the MBC to 94 μg/mL, compared to the cationic homopolymer MBC of 12 μg/mL (~8-fold change). Further increasing PEG_{2k} content significantly abrogated the antibacterial activity, leading to MBC values on the order of some hundreds of μg/mL. Copolymers containing 50 mol% or more of PEG_{2k} are completely inactive against *E. coli* even at the highest concentration tested (1000 μg/mL). The simplest explanation for this trend is that longer PEG_{2k} chains excessively shield the cationic charge and backbone hydrophobicity of the polymers, thus deterring the interaction between polymers and cell membranes to a greater extent than the shorter PEG_{800} chains.

Table 1. Summary of antimicrobial and hemolytic activities of cationic amphiphilic poly(benzyl ether)s as a function of molar percent PEGylation and PEG chain length.

Polymer	mol% PEG	DP*	MBC *E. coli* (μg/mL)	HC_{50} (μg/mL)	HC_{50} / MBC
P_1-100-PEG_{800}	100	10	>1000	>1000	--
P_1-85-PEG_{800}	85	12	>1000	>1000	--
P_1-63-PEG_{800}	63	11	>1000	>1000	--
P_1-57-PEG_{800}	57	11	219	>1000	> 4.6
P_1-50-PEG_{800}	**50**	**12**	**12**	**340**	**28.3**
P_1-33-PEG_{800}	33	12	12	83	6.9
P_1-25-PEG_{800}	25	12	26	89	3.4
P_1-11-PEG_{800}	11	12	26	25	0.96
P_1-100-PEG_{2k}	100	13	>1000	>1000	--
P_1-70-PEG_{2k}	70	13	>1000	>1000	--
P_1-50-PEG_{2k}	50	11	750	>1000	>1.3
P_1-34-PEG_{2k}	34	12	438	>1000	>2.3
P_1-22-PEG_{2k}	22	12	313	234	0.8
P_1-12-PEG_{2k}	12	11	94	46	0.5
P_1-0**	0	13	12	< 8	< 0.7
M_2	100	--	>1000	>1000	--
M_1	0	--	31	62	2
DP_1-50-PEG_{800} (+ CsF)	50	--	8	104	13

*Degree of polymerization (DP) from ^{1}H NMR end group analysis.
**Data from reference[49] for comparison.

It is widely understood that "amphiphilic balance" – finely tuning the interplay of cationic charge to hydrophobic character – is central to the design rationale for antibacterial polymers.[62, 63] Overall, the results here show that PEGylation is an effective strategy to influence the "amphiphilic balance" of cationic, amphiphilic polymers, although judiciously tuning the PEG content and PEG chain length is clearly required. This stands in accord with literature precedent on other polymer platforms.[60, 61] The optimal formulation identified in this work is the copolymer containing ~50% PEG_{800}, which shows improved solubility and slightly enhanced antibacterial activity relative to the cationic PBE homopolymer (**P_1-0**).

We also compared the activity of dye labeled polymers to that of their unlabeled (silyl ether end-capped) counterparts. The MBC values for *RhB*-**P_1-0**, *RhB*-**P_1-40-PEG_{800}** and *RhB*-**P_1-100-PEG_{800}** are 31, 31 and >1000 μg/mL, respectively, which are comparable to **P_1-0**, **P_1-50-PEG_{800}** and **P_1-100-PEG_{800}** (12, 12, and >1000 μg/mL) Thus we conclude that dye itself has only a marginal effect on the antibacterial activity, differing only by a single 2-fold dilution, and therefore these dye-capped polymers are appropriately representative of the polymer library in this work.

Hemolytic activity. The toxicity of these copolymers against mammalian cell membranes is quantified in terms of hemoglobin release from sheep red blood cells (RBCs). The hemolytic concentration (HC_{50}) is defined here as the characteristic polymer concentration that induces 50% hemolysis after 1 h incubation at 37 °C, as determined by curve fitting to the Hill equation. The cationic homopolymer (**P_1-0**) was markedly hemolytic with an HC_{50} value lower than 8 μg/mL, which is comparable to melittin (HC_{50} = 6 μg/mL) in the same assay conditions, in agreement with our recent report.[49] Incorporation of increasing amounts of PEG_{800} monotonically increases the HC_{50} values by orders of magnitude (Table 1 and Figure 4). The

addition of just 11 mol% of PEG_{800} in side chains reduced the hemolytic toxicity by ~ 4-fold (HC_{50} = 25 μg/mL). Further increasing the PEG_{800} content to 25% and 33% mole led to an additional ~3-fold increase in the HC_{50} (89 μg/mL). This trend continued for copolymers containing up to 50 mol% PEG_{800} (HC_{50} = 340 μg/mL). Higher PEG_{800} content led to complete loss of hemolytic activity with HC_{50} values above the highest concentration tested (1000 μg/mL). Cell-type selectivity against bacterial cells without toxicity to mammalian cells is crucial for biomedical-related applications. Comparing the relative magnitudes of HC_{50} and MBC values for the copolymers in this work reveals that the most promising example thus far is the PBE copolymer containing 50% PEG_{800} (HC_{50}/MBC = 28.3). This metric represents a very marked improvement relative to our first-generation self-immolative antibacterial PBE (HC_{50}/MBC = 0.5).[49] Thus, we report the first example of a cell-type selective antibacterial polymer that possesses the unique self-immolative characteristic.

Incorporation of longer grafted PEG_{2k} in side chains exhibited similar effect on hemolytic activity; higher degrees of PEG substitution are associated with loss of hemolytic toxicity in a monotonic manner. The slope of the HC_{50} versus PEG mol% plot (Figure 4) is higher for PEG_{2k} than for PEG_{800}, implying that the longer PEG chains impact the activity more significantly in the low PEG content regime. For example, incorporation of 12 mol% PEG_{2k} gave an HC_{50} value of 46 μg/mL, which is about 6-fold higher than the cationic homopolymer **P_1-0** and about 2-fold less hemolytic than the copolymer containing about the same molar percent of PEG_{800}. Increasing PEG_{2k} mole content to 20% further decreased hemolytic activity. All polymers having 34% or more of PEG_{2k} in the side chains were non-hemolytic even at maximum concentration tested, 1000 μg/mL. Comparing two polymers with similar % mole of PEG, it is obvious that those with longer PEG_{2k} units showed much more hemocompatibility relative to polymer bearing

shorter PEG_{800}. For example, **P_1-34-PEG_{2k}** has an HC_{50} > 1000 μg/mL, compared to **P_1-33-PEG_{800}**, which has HC_{50} = 83 μg/mL (a difference of more than 12-fold). The effect again can be explained by backbone screening by the longer grafted PEG chains, which shields the potent hydrophobicity of the benzyl ether backbone, thus diminishing the interactions with RBC lipid bilayers. Even though polymers with longer PEG side groups are non-hemolytic, they are also less potent antibacterial agents, and hence do not confer excellent selectivity. The best cell-selectivity for a copolymer bearing PEG_{2k} was a modest HC_{50}/MBC > 2.3 for the polymer with 34 mol% PEG_{2k}. This value is far lower than the best example from the PEG_{800} series, which was HC_{50}/MBC = 28.3. It is thus reasonable to speculate that even shorter PEGs may have an even greater effect on the enhancement of selectivity, although at some point the palliative effect is expected to diminish.

In contrast to negatively charged bacterial cell surfaces, the outer leaflet of the phospholipid bilayer in the RBC membrane displays a lower density of anionic charges.[6, 25] The hemolytic behavior of amphiphilic polymers has thus been mostly associated with their hydrophobicity, which results in membrane binding and surfactant-like disruption[64]. The incorporation of hydrophilic PEG side chains plays a prominent role in dictating the hemolytic activity of synthetic polymers. Plasma proteins in blood absorb on RBCs and protect them from external stresses. In the absence of blood plasma, RBCs become more delicate and susceptible to lytic agents (such as in PBS, the assay media used here).[65] PEG also behaves as a protective agent by shielding cells from foreign body contact. It has been shown that PEG weakly absorbs to the cell membrane via hydrogen bonding to improve protection through cells[66]. Consequently, polymers containing PEG may also reduce hemolytic toxicity by these or related mechanisms, in addition to its role in reducing the overall hydrophobicity of the copolymers.

Broad Spectrum and Kinetics. The most promising candidate identified in our initial screen was the copolymer containing 50 mol% PEG_{800} and 50 mol% cysteamine in the side chains, **P_1-50-PEG_{800}**. We further examined the bactericidal profile of this select formulation in terms of broad-spectrum activity and bactericidal kinetics (Figure 5). The copolymer does exert bactericidal activity against both Gram-positive and Gram-negative bacteria. Bactericidal activity is generally more potent in the case of Gram-negatives; the MBC values against *E. coli* and *P. aureginosa* are 12 and 4 μg/mL, respectively, whereas against *S. aureus* and *E. faecalis* the values are 250 and 125 μg/mL. This observation is similar to our previous findings with PBE cationic homopolymers, which exerted much more potent activity against Gram-negatives as compared to Gram-positives. In addition, it was found that the kinetics are slower against Gram- positives, requiring 4-hr incubation to induce a 4-log reduction in the number of viable *S. aureus* cells (99.99% killing) as opposed to less than 1-hr in the case of *E. coli*. It is interesting that these PEGylated PBEs generally show better activity against Gram negative strains relative to Gram positives. Indeed, many examples of antibacterial polymers are more active against Gram-positive bacteria relative to Gram-

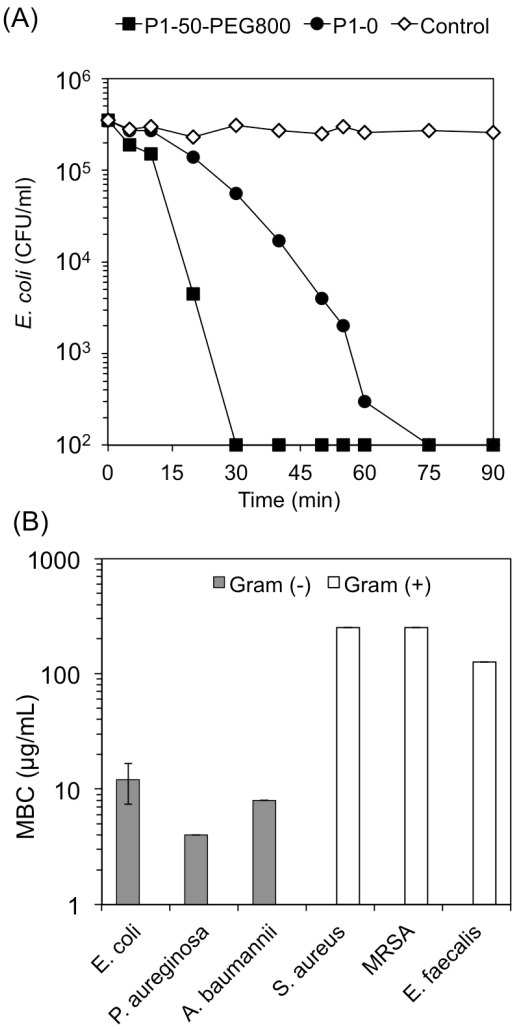

Figure 5. (a) Bactericidal kinetics of **P_1-0** and **P_1-50-PEG_{800}** against *E. coli* in PBS at 2×MBC and (b) Broad spectrum activity against Gram-positive and -negative bacteria.

negatives, although there are also examples that show the opposite preference.[67] A study by Lienkamp *et al* found that there may also be a molecular seiving effect of the peptidoglycan layer in Gram positves.[68] The details of the mechanism of action are outside the scope of this work, but we hypothesize that the thick, cross-linked peptidoglycan layer present in Gram positives may be difficult for these PBE-*graft*-PEG copolymers to translocate.

The PEGylated copolymer **P_1-50-PEG_{800}** exerts markedly faster bactericidal kinetics against *E. coli* (4-log reduction in < 30 min) relative to the cationic homopolymer **P_1-0** (~ 90 min), as shown in Figure 4A. This observation initially seems counterintuitive because the PEGylated copolymer has a lower cationic charge density and lower hydrophobicity, relative to the cationic homopolymer, and the membrane disruption is thought to depend on both electrostatic and hydrophobic interactions. We hypothesized that the PEGylated polymer acts faster overall due to the more subtle hydrophobicity, which disfavors aggregation in solution and thus may facilitate the binding of individually solvated polymer chains onto the bacterial cell envelope. In contrast, the excessively hydrophobic **P_1-0** may exist as aggregates in solution that display cationic groups on the surface and bury the hydrophobic residues in an inner globule. This sort of hydrophobic clustering hypothesis has been invoked to explain the reduced antibacterial activity in the case of excessively hydrophobic polymethacrylates.[69]

To probe our hypothesis, we used the Rhodamine-labeled variants of **P_1-0**, **P_1-50-PEG_{800}**, and **P_1-100-PEG_{800}** each containing one dye tag in the terminal end group (see ESI for synthetic details). The MBC values of these tagged polymers are similar to the untagged polymers of same copolymer composition (data in ESI). Indeed, confocal microscopy images of the *RhB*-**P_1-0** show micron-sized aggregates in PBS buffer at concentrations as low as 16 μg/mL (Figure 6A), which is similar to the MBC value. In stark contrast, *RhB*-**P_1-50-PEG_{800}** and *RhB*-**P_1-100-PEG_{800}** both

show diffuse, uniform fluorescence intensity in PBS even up to 1000 μg/mL, which is well above the MBC value (Figure 6B). Although a detailed study the role of PEGylation in the aggregation process, perhaps using Dynamic Light Scattering (DLS), is outside the scope of this work, it may be an interesting topic for further study of antibacterial SIMPs.

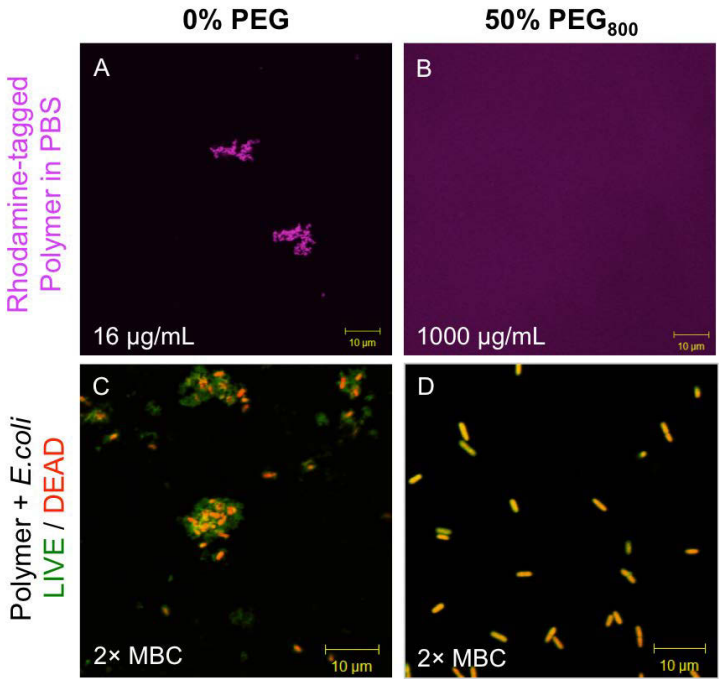

Figure 6. Confocal images of (A, B) rhodamine dye-labeled polymers in PBS media and (C, D) non-labeled polymers at 2x MBC with *E. coli* and LIVE/DEAD stains.

Moreover, when the Rhodamine-labeled polymers are mixed with *E. coli* cells, there is a very clear localization of *RhB*-**P$_1$-50-PEG$_{800}$** specifically on the cell membrane observed in the confocal images (Figure 7A). In contrast, when *RhB*-**P$_1$-0** is mixed with the *E. coli* cells, aggregates on the order of 10s of microns are observed, with no clear individual rod-shaped bacteria cells (Figure 7B). These data strongly support the notion that the activity of the cationic homopolymer **P$_1$-0** is indeed hampered by extensive polymer-polymer aggregation in aqueous media, as we expected. The PEGylation strategy indeed alleviates the excessive hydrophobicity

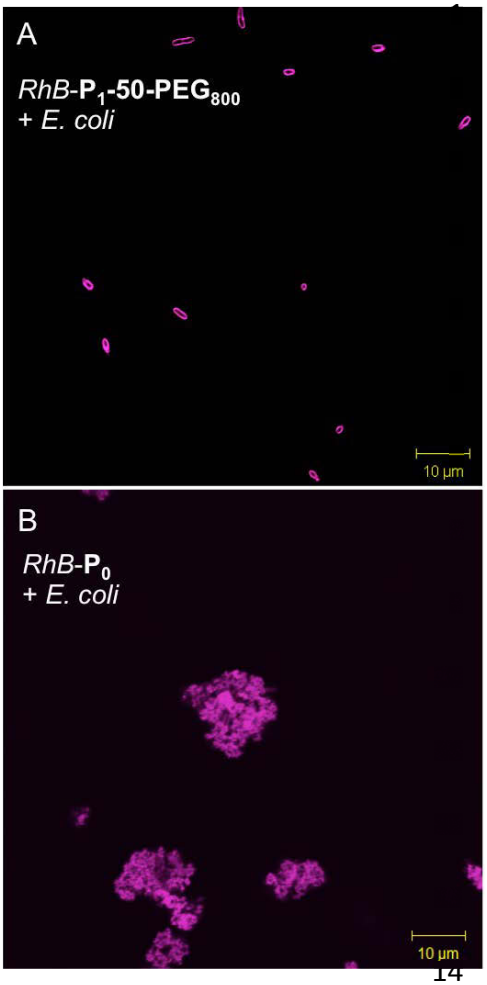

Figure 7. (A) Rhodamine-labeled polymer with 50% PEG_{800} in the side chains binds specifically to the membranes of individual planktonic *E. coli* cells, seen as bright emission from the outlines of smooth rod-shaped cells. (B) Rhodamine-labeled polymer with no PEG (all cysteamine side chains) shows only indistinct aggregates.

of the PBE backbone and brings the global physiochemical properties of the copolymer into the appropriate range for "amphiphilic balance" required to give favorable biological activity.

Triggered depolymerization. We next examined the influence of specifically triggered depolymerization on the antibacterial and hemolytic activities of PEGylated cationic PBEs. In accord with our prior work, TBDMS-capped pre-polymers (**P_0**) undergo rapid depolymerization to small molecules upon fluoride exposure, evidenced by ^{1}H NMR and GPC[49]. In this work, fluoride was introduced as an exogenous trigger. In general, the PBE platform boasts a great deal of diversity in terms of end-cap/trigger combinations that can be used to mediate self-immolation. The present example was selected for synthetic accessibility and because the fluoride ion is biologically *inactive* against bacterial and human cells. Indeed, we are also interested in expanding this work to include naturally occurring *endogenous* triggering chemistries, perhaps involving natural changes in redox, pH, or enzymatic cues, but these efforts are outside the scope of the present work.

Triggered depolymerization of **P_1-50-PEG_{800}** was initiated by cesium fluoride (CsF) in MeOH or DMF, and monitored by ^{1}H NMR and GPC (Figure 8). Upon F^- treatment, broad

features in the ^{1}H NMR spectra attributed to the PBE backbone disappeared and were replaced by sharp peaks corresponding to small molecule products of depolymerization. The disappearance of the resonance at ~5.5 ppm is used to quantify the percent depolymerization, which was quantitative after stirring overnight (Figure S35, ESI). The GPC trace (in DMF) also shows a corresponding shift to longer retention times, in accord with products of smaller hydrodynamic volume that match the chromatogram for the PEG_{800} grafted monomer $\mathbf{M_2}$. The MBC for intact polymer $\mathbf{P_1\text{-}50\text{-}PEG_{800}}$ was 12 μg/mL. In response to fluoride, $\mathbf{P_1\text{-}50\text{-}PEG_{800}}$ degraded into its small molecule components (referred to as $\mathbf{DP_1\text{-}50\text{-}PEG_{800}}$ in Table 1), which had an MBC value of 8 μg/mL. Thus, the products of depolymerization appeared to exert similar antibacterial activity than the intact polymer. The small change in MBC upon depolymerization is consistent with the observation that the small molecule product of depolymerization containing an ammonium cation is a potent antibacterial agent, although the PEGylated monomer has no antibacterial activity.

We also investigated the biological activities of model small molecule compounds that contain either primary amine ($\mathbf{M_1}$ in Table 1) or PEG_{800} ($\mathbf{M_2}$) attached to a single unit of the bisphenol (chemical structures given in Figure 1) as a standard for comparison. In contrast to the potent antibacterial activity of the primary amine functionalized monomer $\mathbf{M_1}$ (31 μg/mL), the PEGylated monomer $\mathbf{M_2}$ was inactive against *E. coli* up to 1000 μg/mL.

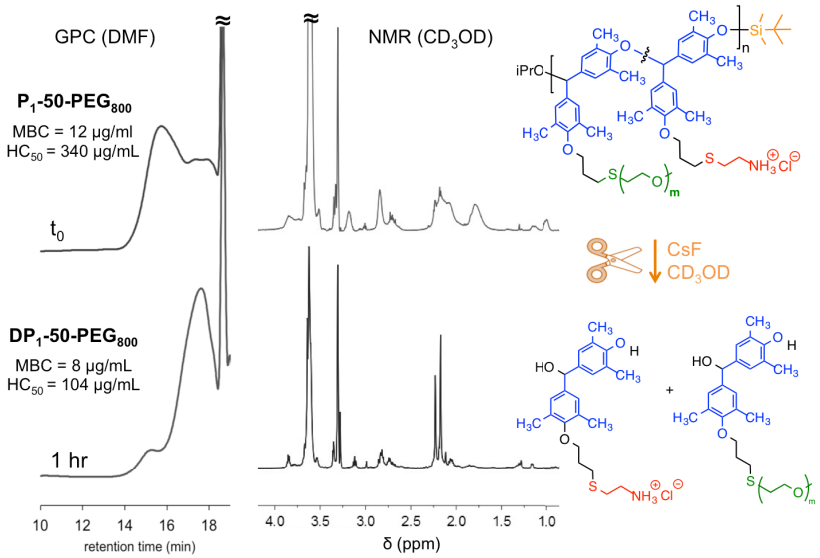

Figure *8*. ^{1}H NMR ($CDOD_3$) and GPC (DMF) of P_1-50-PEG_{800} before and after CsF in MeOH, with their corresponding chemical structures and biological activities.

Triggered self-immolation also influences the hemolytic activity compared to intact polymer. For example, **P_1-50-PEG_{800}** (HC_{50} = 340 μg/mL) depolymerized into **DP_1-50-PEG_{800}** (HC_{50} = 104 μg/mL), about a 3-fold change. This result can be understood in terms of the HC_{50} values for the two monomer components: 62 μg/mL for $\mathbf{M_1}$ and >1000 μg/ml for $\mathbf{M_2}$. If one considers that the two are present in approximately a 1:1 ratio (for this 50-50% copolymer), and that one component is completely inactive, then we expect the simple mixture to have an HC_{50} value that is simply double that of the active component (2 × 62 = 124 μg/mL). The experimental result is 104 μg/mL, which is in reasonably good agreement with the prediction for a simple mixture. Slight differences may be due to the presence of some amount of dimeric species, which has been observed previously in the depolymerization byproducts for PBE.[49]

In addition to the MBC assay that quantified cell death in terms of the number of viable colonies observable to the unaided eye, we also evaluated the antibacterial activity of polymers and its small components by confocal laser scanning microscopy to visualize the antibacterial

effect at the individual cell level, before and after depolymerization (Figure 9).

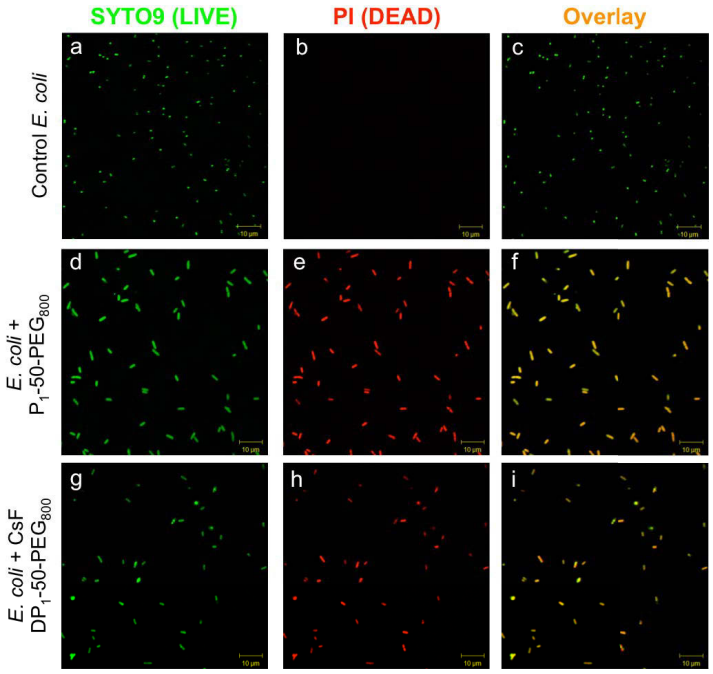

Figure 9. Confocal images of *E. coli* cells (a−c) alone, (d-f) after exposure to **P_1-50-PEG$_{800}$**, (g-i) after exposure to CsF-depolymerization products **DP_1-50-PEG$_{800}$**. Scale bar is 10 μm in all images. Additional images of cells treated with **M_1** and **M_2** are in the SI.

For this study, we employed the commercially-available BacLight LIVE/DEAD staining kit, which includes the proprietary SYTO9 dye (green) that stains both live and dead cells indiscriminately, and propidium iodide (PI, red) that emits only when intercalated into DNA within the cytoplasm.[70] PI staining is thus used as a metric to confirm the permeabilization of the cell membrane, which is the putative mechanism of action for cationic, amphiphilic antibacterial agents.[71-75] Firstly, as a positive control, *E. coli* cells in the absence of polymers were examined. In confocal images, we observed smooth, rod-shaped *E. coli* cells in the green SYTO9 channel with no detectable emission in the red PI channel, which suggests healthy live cells (Figure 9 a-c). To assess the impact of the polymers, *E. coli* (5×10^7 CFU/mL) was incubated for 90 min at 37 °C in the presence of antibacterial polymers above their lethal concentration (4×MBC). We

examined both the intact copolymer **P_1-50-PEG_{800}** (Figure 9 d-f) as well as the products of the triggered depolymerization **DP_1-50-PEG_{800}** (Figure 9 g-i). Both samples showed bright emission in the green and red channels, suggesting substantial co-localization of both fluorophores within the cells.

Based on the fact that the PI stain cannot translocate healthy cell membranes, combined with specific membrane stained by our Rh-labeled polymers, we conclude that DNA-intercalated PI stain within the cytoplasm is associated with a deterioration of the cell membrane barrier function upon exposure to antibacterial polymers. Thus, it would appear that the polymers in this work are capable of permeabilizing the *E. coli* cells, in accord with numerous other literature examples on cationic, amphiphilic polymers.[71-75]

The primary amine functionalized model monomer **M_1** also showed extensive PI staining within the cells (images in ESI). On the other hand, monomer with PEG_{800} functionality **M_2** did not induce any red PI emission from cells, which again confirms that the PEG_{800} monomer units are not bactericidal (images in ESI**)**. Interestingly, the confocal images in this work are rather different in appearance relative to our previous report on the cationic homopolymer. Whereas **P_1-0** showed red PI staining of large cell-cell aggregates on the order of several tens of microns (Figure 6C),[49] the PEGylated variants in the present study appear to stain cells individually without inducing extensive cell-cell aggregation (Figure 6D and 7B), which is also consistent with the concept of reduced hydrophobicity (more negative logP values) for the PEGylated polymers.

Control Experiments. The CsF was not removed prior to testing the biological activity; CsF showed no effect on *E. coli* cell viability even at concentrations 10× higher than present in the assays. As a negative control for triggering, PBEs were end-capped with inert methyl groups,

side-chain functionalized and exposed to CsF under same conditions. The fluoride-triggered depolymerization did not occur in those polymers, evidenced by ^{1}H NMR, and tested for MBC and HC_{50}. Before and after CsF exposure, MBC and HC_{50} values did not show any significant changes. Hence, we confirmed that fluoride-triggered depolymerization is specific to silyl ether end-capped polymers. In addition, we confirmed that no adverse side reactions occur when the allyl functionalized pre-polymer $\mathbf{P_0}$ is exposed to cysteamine (or PEG-SH) under UV irradiation with no photoinitiator present. Similarly, no reaction is observed when $\mathbf{P_0}$ and photoinitiator under UV irradiation without any thiol present.

Experimental

Materials and Methods. Reagents were purchased commercially and used as received without further purification unless noted. 4,4'-methylenebis(2,6-dimethylphenol) was purchased from Tokyo Chemical Industry (TCI America, USA). Potassium carbonate (K_2CO_3), allyl bromide (allyl Br), ammonium chloride (NH_4Cl), sodium chloride (NaCl), anhydrous sodium sulfates (Na_2SO_4), silver oxide (Ag_2O), tert-butyldimethylsilyl chloride (TBDMS-Cl), imidazole, 2-aminoethanethiol hydrochloride (cysteamine), poly(ethylene glycol) methyl ether thiol (M_n = 800g/mole and M_n= 2000 g/mole), 2,2- dimethoxy-2-phenylacetophenone (DMPA), cesium fluoride (CsF), Triton X-100, sodium phosphate monobasic monohydrate and sodium phosphate dibasic heptahydrate were purchased from Sigma-Aldrich (USA). 1-tert-Butyl-2,2,4,4,4-pentakis(dimethylamino)-2λ^5,4λ^5-catenadi(phosphazene) (P_2-*t*-Bu base) (2.0 M solution in THF) was also purchased from Sigma-Aldrich and stored in a glove box under N_2 atmosphere. BacLight^{TM} Bacterial Viability Kit L-7007 and NHS-Rhodamine (5/6-carboxy-tetramethyl-rhodamine succinimidyl ester) were purchased from Thermo Fisher Scientific (USA). 10% (v/v) red blood cells (RBCs) was obtained from MP Biomedicals (USA). Organic solvents: diethyl ether (Et_2O), N,N-dimethylformamide (DMF), ethyl acetate, hexane, methanol (MeOH), and dimethyl sulfoxide (DMSO) were obtained from Sigma-Aldrich (USA). Isopropanol (iPrOH) was distilled before use. Anhydrous tetrahydrofuran (THF) was obtained from solvent purification system. Deionized water was purified using EDM Millipore purification system. Sephadex LH-20 was obtained from Sigma-Aldrich. Flash-column chromatography was

employed using silica gel (60 Å pore size, 40-63 μm technical grade, Sigma-Aldrich). Thin-layer chromatography was performed on IB2-F J.T. Baker silica gel TLC (Germany).

Proton nuclear magnetic resonance (^{1}H NMR) spectra were recorded using 500 MHz Agilent NMR spectrometer at 25 °C. NMR chemical shifts were reported in parts per million (ppm, δ) and referenced to tetramethylsilane ($(CH_3)_4Si$, 0.00 ppm) or to residual solvent signals ($CDCl_3$ (δ 7.27), $(CD_3)_2OS$ (δ 2.50), or CD_3OD (δ 3.31 and 4.78). Carbon nuclear magnetic resonance (^{13}C NMR) spectra were recorded using 500 MHz Agilent NMR spectrometer at 25 °C. NMR chemical shifts were reported in parts per million (ppm, δ) and referenced to residual solvent signals ($CDCl_3$ (δ 77.0), or CD_3OD (δ 49.0).

Size exclusion chromatography (SEC) was performed on Agilent Technologies 1260 Infinity GPC system equipped with a refractive index detector and PLGel columns using THF and DMF as the mobile phase (flow rate: 1 mL/min, 25 °C for THF, flow rate: 1 mL/min, 45 °C for DMF). Molecular weight was calibrated using monodisperse polystyrene standards.

Laser scanning confocal microscopy (Zeiss LSM 510 Meta) was employed using Argon (458-488-514 nm) and HeNe1 (543 nm) lasers. 512 x 512 pixel images were recorded from single scan.

Mass spectra were measured on Thermo LTQ XL Orbitrap mass spectrometer (Thermo, Bremen, Germany) with electrospray ionization ion source. Samples were injected using an Agilent 1200 nano-HPLC system (Agilent, Palo Alto, CA) using an Agilent 1200 autosampler. The flow rate of the solvent was 50 μL/min. The injection volume was 1-2 μL. The data were collected in m/z range of 100-900 at the resolution of 30,000. The accuracy of mass measurements was ~3 ppm.

Monomer Synthesis. Allyl Br (1.0 equiv) was added dropwise to a stirred mixture of 4,4'-methylenebis(2,6-dimethylphenol) (1.0 equiv) and K_2CO_3 (1.1 equiv) in DMF (0.4 M). After 24 h reaction at room temperature, the mixture was extracted with ethyl acetate and deionized H_2O. The organic layer was washed with saturated NH_4Cl solution and then brine. It was dried over anhydrous Na_2SO_4, filtered to separate salts and concentrated via rotary evaporation. On TLC plate, there were three spots observed, assigned to compounds with double allyl and single allyl in the side chains, and unreacted starting material. The viscous oil was purified by silica gel column chromatography with gradient elution of solvents (10 – 33% ethyl acetate in hexanes) to afford compound with **single allyl** as a yellow oil (yield 28%).

Ag_2O (2.0 equiv) was added into the solution of **single allyl** compound (1.0 equiv) and Et_2O (0.1 M). The

reaction was stirred for 16 h at room temperature. The mixture was filtered to remove silver oxide particles, concentrated via rotary evaporator and recrystallized in hot cyclohexane to afford yellow crystals. The monomer $\mathbf{M_0}$ crystals were ground and dried in vacuum for 72 h. Dry monomer (67%) was store in an inert glovebox atmosphere.

Polymer Synthesis. The monomer $\mathbf{M_0}$ (1.0 equiv) was dissolved in anhydrous THF. A stock solution of distilled iPrOH (0.1 equiv) and 2.0 M P_2-*t*-Bu base solution (0.1 equiv) in THF was prepared in anhydrous THF (1:1 ratio). The chain length of polymer was tuned by altering the number of equivalents of initiator relative to monomer. Based on that, certain amount of initiator-base stock solution was added into monomer solution to pre-initiate and stirred for 1 h at room temperature. Final concentration of reaction was adjusted to 0.8 M. The reaction became dark red from bright yellow color after the addition of base. Following the initiation, polymerization was conducted in -20 °C for 4 h with stirring. All steps were carried out in glovebox under inert N_2 environment.

End-capping. TBDMS-Cl (1.0 equiv) and imidazole (1.0 equiv) were dissolved in anhydrous THF and then injected into polymer reaction at -20 °C which immediately turned into orange-yellow color from dark red. Reaction was stirred for 24 h at -20 °C. It was allowed to warm to room temperature and continued to stir at this temperature for few hours. The polymer was precipitated in MeOH and collected via centrifuge. Excess MeOH was decanted. The polymer was redissolved in THF and precipitated in MeOH and centrifuged again, whole process was repeated three times. Polymers were dried in vacuum for 24 h. Yields for each polymerization are given in the ESI.

Synthetic procedures largely followed the precedent by Phillips,[50] and our own prior report,[49] with minor modifications. Further synthetic details, triggered depolymerization, NMR and GPC data, biological assay protocols, and microscopy procedures, are included in the Electronic Supporting Information (ESI) document.

Conclusions

We functionalized the side chains of a self-immolative poly(benzyl ether) with a combination of cationic ammonium groups and neutral, hydrophilic PEG chains. The antibacterial and hemolytic activity of these copolymers is sensitively dependent on the cationic charge and hydrophobicity of the polymer chains. Here, we find that side chain PEGylation is a highly effective strategy to modulate the hydrophobicity and to enhance cell-type selectivity. The

copolymer composition (molar percentage of PEG grafts) and the PEG chain length are key design parameters for tuning biological activity. From our library of PBE copolymers, the most promising example is one that contains 50 mol% PEG_{800} and 50 mol% primary ammonium cationic side chains. This select example exerts excellent 28-fold selectivity for bacterial cells relative to mammalian RBCs. The sensitive and specific self-immolative characteristics of the backbone are retained upon side chain functionalization.

In this work, we used stimuli-responsive end-caps that are cleaved on demand by externally applied stimulus, like fluoride ions. The beauty of the self-immolative PBE platform is that these polymers can be designed with a variety of responsive groups, triggered by light, pH, or redox. Currently, we are developing biologically active degradable macromolecules that can be degraded by naturally occurring stimuli including bacterial enzymes. We envision these materials may be useful in a broad range of antibacterial and antibiofilm coatings with unique "triggered-cleaning" characteristics. These and related studies are currently underway in our laboratory.

Acknowledgements

We thank Prof. Scott Phillips for helpful discussions on self-immolative polymer synthesis, Prof. Sangwoo Lee and Prof. Chulsung Bae for the use of GPC, Dr. Ao Chen for helpful discussions, and undergraduate students Samuel Ellman, Sadjo Sidikou, and Phillip Falcone for their assistance with the synthesis and scale-up of the monomers used in this study. E.F.P. acknowledges funding from a 3M Non-Tenured Faculty Award, a National Science Foundation CAREER Award (DMR BMAT #1653418), and the American Chemical Society Petroleum Research Fund (57806-DNI7). C.E. was supported in part by a Presidential Graduate Research

Fellowship from Rensselaer Polytechnic Institute.

ToC Graphic:

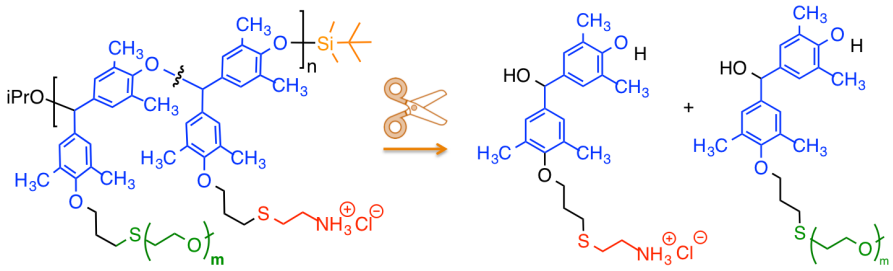

References

1. H. W. Boucher, G. H. Talbot, J. S. Bradley, J. E. Edwards, D. Gilbert, L. B. Rice, M. Scheld, B. Spellberg and J. Bartlett, *Clin Infect Dis*, 2009, **48**, 1-12.
2. H. C. Neu, *Science*, 1992, **257**, 1064-1073.
3. J. Rello, E. Bunsow and A. Perez, *Expert Rev Clin Phar*, 2016, **9**, 1547-1555.
4. M. Zasloff, *Nature*, 2002, **415**, 389-395.
5. T. Ganz, *Nature*, 2001, **412**, 392-393.
6. R. E. W. Hancock and H. G. Sahl, *Nat Biotechnol*, 2006, **24**, 1551-1557.
7. E. A. Porter, X. F. Wang, H. S. Lee, B. Weisblum and S. H. Gellman, *Nature*, 2000, **404**, 565-565.
8. J. A. Patch and A. E. Barron, *Journal of the American Chemical Society*, 2003, **125**, 12092-12093.
9. B. P. Mowery, S. E. Lee, D. A. Kissounko, R. F. Epand, R. M. Epand, B. Weisblum, S. S. Stahl and S. H. Gellman, *Journal of the American Chemical Society*, 2007, **129**, 15474-+.
10. K. Kuroda and W. F. DeGrado, *J Am Chem Soc*, 2005, **127**, 4128-4129.
11. E. F. Palermo and K. Kuroda, *Biomacromolecules*, 2009, **10**, 1416-1428.
12. E. F. Palermo, S. Vemparala and K. Kuroda, *Biomacromolecules*, 2012, **13**, 1632-1641.
13. E. F. Palermo, I. Sovadinova and K. Kuroda, *Biomacromolecules*, 2009, **10**, 3098-3107.
14. W. Chin, G. S. Zhong, Q. Q. Pu, C. Yang, W. Y. Lou, P. F. De Sessions, B. Periaswamy, A. Lee, Z. C. Liang, X. Ding, S. J. Gao, C. W. Chu, S. Bianco, C. Bao, Y. W. Tong, W. M. Fan, M. Wu, J. L. Hedrick and Y. Y. Yang, *Nat Commun*, 2018, **9**.
15. W. Chin, C. A. Yang, V. W. L. Ng, Y. Huang, J. C. Cheng, Y. W. Tong, D. J. Coady, W. M. Fan, J. L. Hedrick and Y. Y. Yang, *Macromolecules*, 2013, **46**, 8797-8807.
16. A. C. Engler, J. P. K. Tan, Z. Y. Ong, D. J. Coady, V. W. L. Ng, Y. Y. Yang and J. L. Hedrick, *Biomacromolecules*, 2013, **14**, 4331-4339.
17. F. Nederberg, Y. Zhang, J. P. K. Tan, K. J. Xu, H. Y. Wang, C. Yang, S. J. Gao, X. D. Guo, K. Fukushima, L. J. Li, J. L. Hedrick and Y. Y. Yang, *Nature Chemistry*, 2011, **3**, 409-414.
18. M. F. Ilker, K. Nusslein, G. N. Tew and E. B. Coughlin, *J Am Chem Soc*, 2004, **126**, 15870-15875.
19. G. J. Gabriel, J. A. Maegerlein, C. E. Nelson, J. M. Dabkowski, T. Eren, K. Nusslein and G. N. Tew, *Chem-Eur J*, 2009, **15**, 433-439.
20. K. Lienkamp and G. N. Tew, *Chem-Eur J*, 2009, **15**, 11784-11800.
21. C. Ergene, K. Yasuhara and E. F. Palermo, *Polym Chem-Uk*, 2018, **9**, 2407-2427.
22. Y. C. Yang, Z. G. Cai, Z. H. Huang, X. Y. Tang and X. Zhang, *Polym J*, 2018, **50**, 33-44.
23. W. Ren, W. R. Cheng, G. Wang and Y. Liu, *J Polym Sci Pol Chem*, 2017, **55**, 632-639.
24. M. Hartlieb, E. G. L. Williams, A. Kuroki, S. Perrier and K. E. S. Locock, *Curr Med Chem*, 2017, **24**, 2115-2140.
25. K. A. Brogden, *Nat Rev Microbiol*, 2005, **3**, 238-250.
26. H. G. Boman, *Immunological Reviews*, 2000, **173**, 5-16.
27. I. Sovadinova, E. F. Palermo, M. Urban, P. Mpiga, G. A. Caputo and K. Kuroda, *Polymers*, 2011, **3**, 1512-1532.
28. A. K. Marr, W. J. Gooderham and R. E. W. Hancock, *Current Opinion in Pharmacology*, 2006, **6**, 468-472.
29. G. N. Tew, R. W. Scott, M. L. Klein and W. F. Degrado, *Accounts Chem Res*, 2010, **43**, 30-39.
30. A. C. Engler, N. Wiradharma, Z. Y. Ong, D. J. Coady, J. L. Hedrick and Y. Y. Yang, *Nano Today*, 2012, **7**, 201-222.
31. H. Takahashi, G. A. Caputo, S. Vemparala and K. Kuroda, *Bioconjugate Chem*, 2017, **28**, 1340-1350.
32. M. Mizutani, E. F. Palermo, L. M. Thoma, K. Satoh, M. Kamigaito and K. Kuroda, *Biomacromolecules*, 2012, **13**, 1554-1563.
33. E. A. Chamsaz, S. Mankoci, H. A. Barton and A. Joy, *ACS Appl Mater Inter*, 2017, **9**, 6704-6711.
34. V. W. L. Ng, J. P. K. Tan, J. Y. Leong, Z. X. Voo, J. L. Hedrick and Y. Y. Yang, *Macromolecules*, 2014, **47**, 1285-1291.
35. D. N. Amato, D. V. Amato, O. V. Mavrodi, W. B. Martin, S. N. Swilley, K. H. Parsons, D. V. Mavrodi and D. L. Patton, *ACS Macro Lett*, 2017, **6**, 171-175.
36. M. Vert, *Biomacromolecules*, 2005, **6**, 538-546.
37. A. Sagi, R. Weinstain, N. Karton and D. Shabat, *J Am Chem Soc*, 2008, **130**, 5434-+.
38. S. T. Phillips and A. M. DiLauro, *ACS Macro Lett*, 2014, **3**, 298-304.
39. G. I. Peterson, M. B. Larsen and A. J. Boydston, *Macromolecules*, 2012, **45**, 7317-7328.

40. A. D. Wong, M. A. DeWit and E. R. Gillies, *Adv Drug Deliver Rev*, 2012, **64**, 1031-1045.
41. B. Fan, J. F. Trant, A. D. Wong and E. R. Gillies, *J Am Chem Soc*, 2014, **136**, 10116-10123.
42. M. Shamis, H. N. Lode and D. Shabat, *J Am Chem Soc*, 2004, **126**, 1726-1731.
43. H. Wang, Q. Huang, H. Chang, J. R. Xiao and Y. Y. Cheng, *Biomater Sci-Uk*, 2016, **4**, 375-390.
44. Y. Xie, T. Murray-Stewart, Y. Z. Wang, F. Yua, J. Li, L. J. Marton, R. A. Casero and D. Oupicky, *J Control Release*, 2017, **246**, 110-119.
45. A. M. DiLauro, G. G. Lewis and S. T. Phillips, *Angew Chem Int Edit*, 2015, **54**, 6200-6205.
46. H. Zhang, K. Yeung, J. S. Robbins, R. A. Pavlick, M. Wu, R. Liu, A. Sen and S. T. Phillips, *Angew Chem Int Edit*, 2012, **51**, 2400-2404.
47. A. P. Esser-Kahn, S. A. Odom, N. R. Sottos, S. R. White and J. S. Moore, *Macromolecules*, 2011, **44**, 5539-5553.
48. M. S. Baker, H. Kim, M. G. Olah, G. G. Lewis and S. T. Phillips, *Green Chem*, 2015, **17**, 4541-4545.
49. C. Ergene and E. F. Palermo, *Biomacromolecules*, 2017, **18**, 3400-3409.
50. M. G. Olah, J. S. Robbins, M. S. Baker and S. T. Phillips, *Macromolecules*, 2013, **46**, 5924-5928.
51. K. Yeung, H. Kim, H. Mohapatra and S. T. Phillips, *J Am Chem Soc*, 2015, **137**, 5324-5327.
52. K. Hu, N. W. Schmidt, R. Zhu, Y. J. Jiang, G. H. Lai, G. Wei, E. F. Palermo, K. Kuroda, G. C. L. Wong and L. H. Yang, *Macromolecules*, 2013, **46**, 1908-1915.
53. X. Yang, K. Hu, G. T. Hu, D. Y. Shi, Y. J. Jiang, L. W. Hui, R. Zhu, Y. T. Xie and L. H. Yang, *Biomacromolecules*, 2014, **15**, 3267-3277.
54. S. Chakraborty, R. H. Liu, Z. Hayouka, X. Y. Chen, J. Ehrhardt, Q. Lu, E. Burke, Y. Q. Yan, B. Weisblum, G. C. L. Wong, K. S. Masters and S. H. Gellman, *J Am Chem Soc*, 2014, **136**, 14530-14535.
55. M. Alvarez-Paino, A. Munoz-Bonilla, F. Lopez-Fabal, J. L. Gomez-Garces, J. P. A. Heuts and M. Fernandez-Garcia, *Biomacromolecules*, 2015, **16**, 295-303.
56. E. H. H. Wong, M. M. Khin, V. Ravikumar, Z. Y. Si, S. A. Rice and M. B. Chan-Park, *Biomacromolecules*, 2016, **17**, 1170-1178.
57. S. Colak, C. F. Nelson, K. Nusslein and G. N. Tew, *Biomacromolecules*, 2009, **10**, 353-359.
58. A. Punia, A. Mancuso, P. Banerjee and N. L. Yang, *ACS Macro Lett*, 2015, **4**, 426-430.
59. A. Punia, K. Lee, E. He, S. Mukherjee, A. Mancuso, P. Banerjee and N. L. Yang, *Int J Mol Sci*, 2015, **16**, 23867-23880.
60. B. C. Allison, B. M. Applegate and J. P. Youngblood, *Biomacromolecules*, 2007, **8**, 2995-2999.
61. P. H. Sellenet, B. Allison, B. M. Applegate and J. P. Youngblood, *Biomacromolecules*, 2007, **8**, 19-23.
62. E. F. Palermo and K. Kuroda, *Appl Microbiol Biot*, 2010, **87**, 1605-1615.
63. H. Takahashi, E. F. Palermo, K. Yasuhara, G. A. Caputo and K. Kuroda, *Macromol Biosci*, 2013, **13**, 1285-1299.
64. K. Kuroda and G. A. Caputo, *Wires Nanomed Nanobi*, 2013, **5**, 49-66.
65. M. V. Kameneva, J. F. Antaki, K. K. Yeleswarapu, M. J. Watach, B. P. Griffith and H. S. Borovetz, *Asaio Journal*, 1997, **43**, M571-M575.
66. M. V. Kameneva, B. M. Repko, E. F. Krasik, B. C. Perricelli and H. S. Borovetz, *Asaio Journal*, 2003, **49**, 537-542.
67. K. Lienkamp, A. E. Madkour, A. Musante, C. F. Nelson, K. Nuesslein and G. N. Tew, *J Am Chem Soc*, 2008, **130**, 9836-9843.
68. K. Lienkamp, K. N. Kumar, A. Som, K. Nusslein and G. N. Tew, *Chem-Eur J*, 2009, **15**, 11710-11714.
69. K. Kuroda, G. A. Caputo and W. F. DeGrado, *Chem-Eur J*, 2009, **15**, 1123-1133.
70. P. Stiefel, S. Schmidt-Emrich, K. Maniura-Weber and Q. Ren, *Bmc Microbiol*, 2015, **15**.
71. L. H. Yang, V. D. Gordon, D. R. Trinkle, N. W. Schmidt, M. A. Davis, C. DeVries, A. Som, J. E. Cronan, G. N. Tew and G. C. L. Wong, *P Natl Acad Sci USA*, 2008, **105**, 20595-20600.
72. H. Choi, S. Chakraborty, R. H. Liu, S. H. Gellman and J. C. Weisshaar, *ACS Chem Biol*, 2016, **11**, 113-120.
73. S. Hovakeemian, R. H. Liu, S. H. Gellman and H. Heerklotz, *Biophys J*, 2015, **108**, 551a-551a.
74. S. G. Hovakeemian, R. H. Liu, S. H. Gellman and H. Heerklotz, *Soft Matter*, 2015, **11**, 6840-6851.
75. E. F. Palermo, D.-K. Lee, A. Ramamoorthy and K. Kuroda, *J Phys Chem B*, 2011, **115**, 366-375.